TU Delft

Delft University of Technology

Simulation models for the minimum velocity for foam generation and propagation

Yu, G.; Rossen, W.R.

DOI
10.1016/j.petrol.2022.110406

Publication date
2022

Document Version
Final published version

Published in
Journal of Petroleum Science and Engineering

Citation (APA)
Yu, G., & Rossen, W. R. (2022). Simulation models for the minimum velocity for foam generation and propagation. *Journal of Petroleum Science and Engineering*, *214*, Article 110406. https://doi.org/10.1016/j.petrol.2022.110406

Important note
To cite this publication, please use the final published version (if applicable).
Please check the document version above.

Copyright
Other than for strictly personal use, it is not permitted to download, forward or distribute the text or part of it, without the consent of the author(s) and/or copyright holder(s), unless the work is under an open content license such as Creative Commons.

Takedown policy
Please contact us and provide details if you believe this document breaches copyrights.
We will remove access to the work immediately and investigate your claim.

This work is downloaded from Delft University of Technology.
For technical reasons the number of authors shown on this cover page is limited to a maximum of 10.

Journal of Petroleum Science and Engineering 214 (2022) 110406

Contents lists available at ScienceDirect

Journal of Petroleum Science and Engineering

journal homepage: www.elsevier.com/locate/petrol

Simulation models for the minimum velocity for foam generation and propagation

G. Yu, W.R. Rossen *

Dept. of Geoscience and Engineering, Delft University of Technology, Stevinweg 1, 2628, CN, Delft, the Netherlands

ARTICLE INFO

Keywords:
Foam for enhanced oil recovery (EOR)
Foam for CO_2/H_2 storage
Foam generation
Foam propagation
Foam simulation models
Numerical reservoir simulation

ABSTRACT

Foam injection is a promising means of reducing the relative mobility of gas, and hence improving the sweep efficiency of gas, in CO_2 and H_2 storage, soil-contaminant removal in aquifer remediation, enhanced oil recovery, and matrix-acid well stimulation. Theory (Rossen and Gauglitz, 1990; Ashoori et al., 2012) and experiments (Gauglitz et al., 2002; Yu et al., 2019, 2020) indicate that both foam generation and propagation in steady flow in porous media require the attainment of a sufficiently large superficial velocity or pressure gradient ∇P. Here we examine several foam-simulation models for their ability to represent a minimum velocity, or trigger, for foam generation. We define criteria for representation of such a trigger. For simplicity, we assume a homogeneous porous medium and absence of an oleic phase. We examine the Population-Balance (PB) models of Kam and Rossen (2003) and one of its variants (Kam, 2008), and the PB model of Chen et al. (2010); and the implicit-texture (IT) models in CMG-STARS (Computer Modeling Group, 2017) and of Lotfollahi et al. (2017).

Our result show that the PB models of Kam and Rossen and its variant, and the IT models of CMG-STARS and of Lotfollahi et al. do represent a minimum velocity for foam generation. They achieve this by modeling an abrupt decrease in gas mobility with increasing pressure gradient over some range of ∇P. The model of Chen et al. (2010) is based on the model of Kovscek and Radke (1996), which was not intended to represent a trigger for foam generation (Kovscek and Radke, 1993). We cannot say categorically whether it could predict a trigger for any set of model parameter values. Instead, we derive criteria that must be satisfied by the choice of parameters to represent a trigger for foam generation.

In simulations of radial foam propagation the STARS foam model predicts that foam propagation fails at the radius at which local ∇P cannot maintain strong foam, not at a greater velocity and ∇P as seen in experiments (Yu et al., 2020). In addition, we identify a fundamental challenge in representing foam generation at the large ∇P at the wellbore in a numerical simulation: conventional simulators do not represent ∇P at the wellbore. Foam generation at the very high superficial velocity at the well radius is not represented in the absence of truly exceptional grid refinement.

CRediT statement

William Rossen: Conceptualization, Writing-Editing, Supervision. Guanqun Yu: Software, Validation, Investigation, Writing- original draft, Visualization.

1. Introduction

Injecting foam into geological formations can improve gas-injection improved oil recovery by reducing the relative mobility of the gas, which helps mitigate the unfavourable mobility ratio at the leading edge of gas bank as well as the effects of the unfavourable density ratio between gas and water (Schramm, 1994; Kovscek and Radke, 1994; Rossen, 1996). The impact of foam on gas mobility ultimately leads to a greater sweep efficiency of gas.

Foam in porous media is composed of gas bubbles dispersed in the aqueous phase. The degree to which gas mobility is reduced by foam largely depends on the average bubble size (Falls et al., 1988; Friedmann et al., 1991; Kovscek and Radke, 1994; Rossen, 1996), quantified in the bubble/lamella density (number per unit volume, also referred to as foam texture), n_f. A lamella is a thin liquid film stabilized by surfactant. Previous theory and experimental studies (Rossen and Gauglitz, 1990;

* Corresponding author.
E-mail address: w.r.rossen@tudelft.nl (W.R. Rossen).

https://doi.org/10.1016/j.petrol.2022.110406
Received 9 November 2021; Received in revised form 11 March 2022; Accepted 14 March 2022
Available online 7 April 2022
0920-4105/© 2022 The Authors. Published by Elsevier B.V. This is an open access article under the CC BY license (http://creativecommons.org/licenses/by/4.0/).

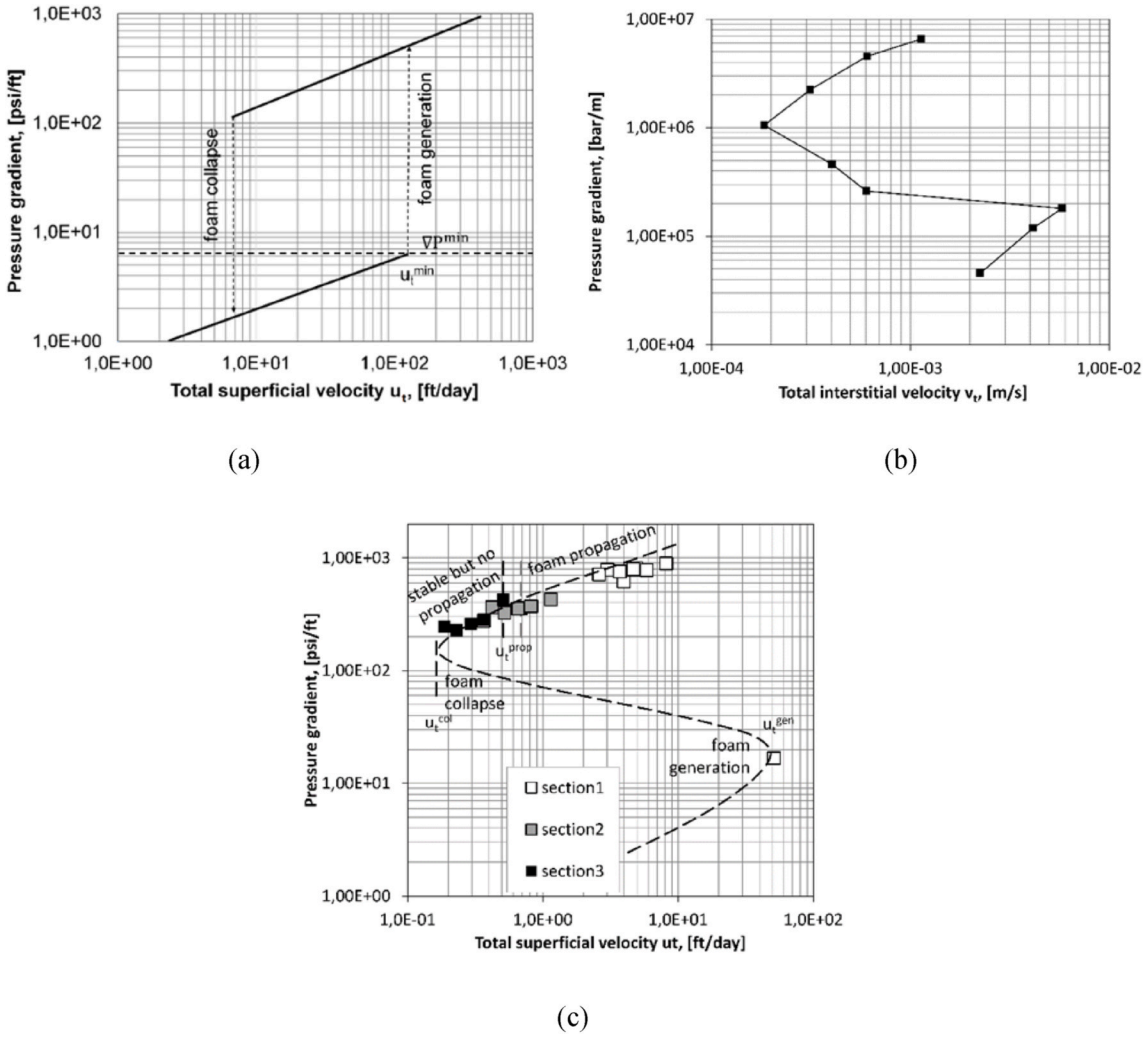

Fig. 1. (a) Schematic of a fixed-rate foam-generation experiment (Gauglitz et al., 2002). The steady state of foam is obtained by fixing total superficial velocity u_t at constant foam quality f_g. These experiments did not specifically verify a minimum velocity for foam collapse. "Foam collapse" here means an abrupt rise in mobility, which could signify a transition to continuous-gas foam (Falls et al., 1988). (b) Data from fixed-ΔP experiment of Gauglitz et al. (2002). In this experiment, pressure difference across the core was raised in a series of steps at a fixed foam quality. The room-temperature coreflood was conducted in Boise sandstone core of permeability 7.1 μm^2, 1.0 wt% SD1000 (alkyl sulfonate) surfactant, in 0.1 wt% NaCl brine. In the intermediate (unstable) state, the authors report, flow rates fluctuated and were difficult to control. (c) Experimentally measured multiple steady states of foam, from Yu et al. (2020). The coreflood was conducted at room temperature (~22 °C) in Bentheimer sandstone core (k = 2.5 μm^2) with N_2 gas and 0.3 wt% BIOTERGE AS-40 (C14-16 alpha olefin sulfonate) surfactant in 3.0 wt% NaCl brine. The vertical dashed lines draw the approximate boundaries for the values of superficial velocities that are crucial to foam.

Gauglitz et al., 2002; Yu et al., 2019) identify a minimum total superficial velocity (related to a minimum pressure gradient) for foam generation in homogeneous porous media. Such experiments begin with steady flow of gas and aqueous phase, which then switches to co-injection of surfactant solution and gas at the same injected gas fraction f_g (also called foam quality). This experimental approach is directly relevant to the field application of steam foam (Friedmann et al., 1994; Patzek, 1996), where steam is usually injected for a long period of time prior to the introduction of surfactant solution at the same gas fraction. It is also key to the issue of foam propagation, including surfactant-alternating-gas (SAG, also known as FAWAG) foam processes, far from an injection well, where gas fractional flow is roughly constant (Stone, 1982).

In this and related studies (Rossen and Gauglitz, 1990; Gauglitz et al., 2002; Kam and Rossen, 2003; Ashoori et al., 2012; Yu et al., 2019), *foam generation* means an abrupt jump from a state of high gas mobility (no/weak foam) to a state of much (e.g., 100 × or more) lower gas mobility (strong foam) upon attaining a sufficiently large total superficial velocity or pressure gradient. In the following text, we express the minimum superficial velocity for foam generation as u_t^{gen}, and the minimum pressure gradient as ∇P^{gen}.

In the experiments of Gauglitz et al. (2002), foam is generated in situ either by fixing total superficial velocity (fixed-rate experiment) (Fig. 1a), or by fixing the pressure drop along the flow direction (fixed-ΔP experiment) (Fig. 1b). Both types of experiments begin with a steady state of no/weak foam at relatively low superficial velocity or pressure gradient. In a fixed-rate experiment (Fig. 1a), superficial velocity is then increased in steps until the minimum superficial velocity u_t^{gen} for foam generation is reached. At u_t^{gen}, pressure drop across the core increases sharply while flow rate remains constant. After a steady state of strong foam is established, foam remains stable at superficial velocities much lower than u_t^{gen}. In fixed-ΔP experiments (Fig. 1b), pressure drop across the core is increased in steps instead of superficial velocity. At u_t^{gen}, superficial velocity decreases with increases in ΔP. These experiments reveal a third (unstable) steady state between the two identified in the fixed-rate experiments. This phenomenon is common in other branches of physics and described by Catastrophe Theory (Zeeman, 1977).

The data in Fig. 1b and c were taken in experiments under ideal conditions for very strong foam (strongly water-wet, high permeability rock, low temperature, low salinity, N_2 gas, etc.). Data in Fig. 1b were for a surfactant/N_2 foam in Boise sandstone (Gauglitz et al., 2002). Data in Fig. 1c are from a surfactant/N_2 foam in Bentheimer sandstone. Therefore the numerical values should not be taken as typical of field application under more-challenging conditions, or with supercritical CO_2 (as discussed further below). The minimum ∇P and velocity for generation were found by Gauglitz et al. (2002) to be much less for CO_2 than for N_2, and CO_2 foam often flows at much lower ∇P than N_2 foam (see, e.g., Chou, 1991).

The dependence of foam generation on pressure gradient is explained by Rossen and Gauglitz (1990) in their network model of foam generation in homogenous porous media. In their model, the underlying mechanism that triggers foam generation is the mobilization and subsequent division of lamellae; the fundamental driving force is pressure gradient instead of velocity. Their percolation model relates the minimum superficial velocity to the pressure difference required to mobilize a lamella in a pore throat. However, since velocity is usually fixed and much easier to control in a foam-generation experiment, one usually reports experimental results in terms of u_t^{gen}. In the model of Rossen and Gauglitz (1990), the threshold condition to trigger lamella division and foam generation depends also on aqueous surface tension and permeability, as well as foam quality. The model fits trends in u_t^{gen} with permeability in sand- and beadpacks and with f_g in sandstone cores, and also predicts much-lower values of u_t^{gen} for supercritical CO_2 foam (with lower surface tension). Their model predicts the trigger for foam generation in steady flow, but doesn't account for the dynamics of foam such as convection, generation and destruction of lamellae after foam generation begins.

Previous experimental studies also suggest a minimum superficial velocity and ∇P for foam propagation. This minimum velocity, if present, could limit foam propagation out to large distances from an injection well in radial flow. The foam-propagation experiments of Friedmann et al. (1994) in a cone-shaped sandpack suggests that foam created near the well at large superficial velocity may not be able to propagate far from the well at much-lower superficial velocity. In the same study, they also report a failure of foam propagation 42 ft from the injection well after 18 months of steam-foam injection, though this conclusion is contested by Patzek (1996). The traveling-wave analysis of Ashoori et al. (2012) shows a connection between the minimum superficial velocity for foam generation and a minimum velocity for foam propagation u_t^{prop}. This u_t^{prop} is greater than the velocity at which foam becomes unstable and collapses u_t^{col}, i.e. where the slope of the upper portion of the plot of ∇P v. u_t in Fig. 1b reverses sign to negative values. In their model, the failure of foam propagation is due to insufficient lamella creation at the leading edge of foam front. Yu et al. (2020) provide experimental evidence for this prediction of Ashoori et al. illustrated in Fig. 1c. They report values for the three threshold superficial velocities u_t^{gen}, u_t^{prop}, and u_t^{col}. If a foam model is able to represent a minimum velocity or trigger for foam generation, this raises the question whether it also predicts minimum velocities for foam propagation and collapse.

This paper reviews current simulation models for foam in porous media, and whether these models can represent a minimum superficial velocity, or minimum pressure gradient, for foam generation. In this study, we do not address the usefulness of these foam models for all applications. Instead, we focus on one facet: the ability of the models to predict an abrupt change of steady state from no/weak foam to strong foam upon a modest increase in total superficial velocity at constant foam quality. If a model can describe a minimum superficial velocity for foam generation, the local-equilibrium solution of the model must be able to represent a sharp jump of state from no-foam to strong-foam upon reaching a threshold value of velocity (Fig. 1a), and the multiple steady states of foam (Fig. 1b), both implied by foam-generation experiments of Gauglitz et al. (2002). In this study, we first specify the criteria and mathematical constraints required to describe a minimum superficial velocity for foam generation. We then examine the structures and formulations of the various foam models alongside the criteria we define.

Our analysis considers both Population-Balance (PB) foam models, where foam texture n_f is represented explicitly, and Implicit-Texture (IT) foam models, where the effects of foam texture are represented implicitly by a factor reducing gas mobility as a function of local conditions. We first examine the PB model of Kam and Rossen (2003) and one of its variants (Kam, 2008). These models have already demonstrated minimum superficial velocities for foam generation and for foam propagation (Ashoori et al., 2012). We also examine the PB model of Chen et al. (2010), a variant of the model introduced by Kovscek and Radke (1996). Among IT foam models, we examine the STARS foam model (Computer Modeling Group) and a modified version of this model proposed by Lotfollahi et al. (2017). In addition, we consider the prediction of the STARS foam model regarding long-distance foam propagation in radial flow, using numerical simulation, and challenges to any model representing foam generation as a function of pressure gradient in numerical simulation.

Finally, we examine the behavior of the models that predict a threshold velocities for foam generation and propagation as a function of key parameters to probe how the thresholds might shift under different conditions, surfactant formulation or gas.

2. Criteria for a minimum superficial velocity for foam generation

Our definition of a trigger for foam generation focuses on pressure gradient ∇P as a function of total superficial velocity u_t at fixed quality f_g, illustrated in Fig. 1. At low ∇P there is a steady state where ∇P increases with u_t. In this state gas mobility is large and foam texture n_f is too small to significantly affect gas mobility. At some point, upon a small increase in u_t, there is an abrupt change of steady state to one with large ∇P and low gas mobility, with significant increases in both gas saturation and capillary pressure. Foam texture in this state is large enough to have a dominant effect on gas mobility. In this regime, again, ∇P is an increasing function of u_t.

The models described below all predict ∇P as a smooth, continuous function of u_t at fixed f_g. This implies the existence of an intermediate regime where

$$\left(\frac{du_t}{d\nabla P}\right)_{f_g} < 0 \tag{1}$$

with

$$u_t = \lambda_t(S_w, \nabla P)\nabla P \tag{2}$$

Eqs. (1) and (2) imply

$$\left(\frac{d\log(\lambda_t(S_w, \nabla P))}{d\log(\nabla P)}\right)_{f_g} < -1 \tag{3}$$

where log represents base-10 logarithm. Since u_t is proportional to ∇P (Eq. (2)), λ_t must decrease with increasing ∇P faster than ∇P increases. We employ these criteria to examine whether a model can predict a minimum velocity or pressure gradient for foam generation.

2.1. Population-balance model of Kam and Rossen (2003)

In the Population-Balance model of Kam and Rossen (2003) and variants of this model (e.g., Kam, 2008), as in other PB models, gas-phase mobility is an explicit function of foam texture n_f. Steady-state foam texture is in turn the result of processes of creation and destruction of lamellae. In the equations below, version (a) is that of Kam and Rossen (2003) and version (b) that of Kam (2008). In these models, the

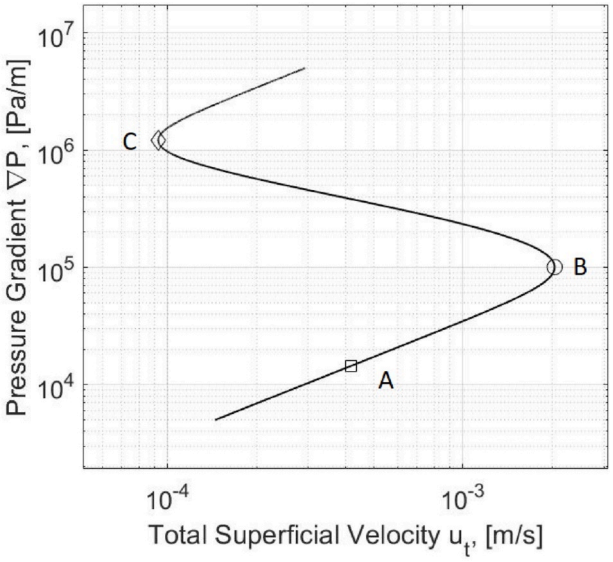

Fig. 2. Local-Equilibrium solution for the Population-Balance model of Kam and Rossen (2003) at foam quality f_g = 91%. B marks the trigger for foam generation. The curve between A and B represents the steady state of weak/no foam; the curve between B and C represents the unstable steady-state of intermediate foam; and the curve above C represents the steady state of strong foam. Parameter values used in this plot are listed in Table A1.

relative permeability of gas k_{rg} is unaffected by the presence of foam and remains a unique function of water saturation S_w. The impact of foam on the reduction of gas-phase mobility is represented as an increase in the viscosity of gas, μ_g^f.

Lamella density is determined by simultaneous processes of lamella creation and destruction. Upon achieving Local Equilibrium (LE), the rate of lamella generation r_g (Eq. (4)) and destruction r_c (Eq. (5)) are equal (Eq. (6)), and bubble density arrives at its equilibrium value $n_{f,LE}$. The rate of lamella generation r_g is function of pressure gradient ∇P (Eq. (4)), with the specific function differing in the two models. Lamella coalescence depends on foam texture and water saturation (Eq. (5)). The impact of capillary pressure is not explicitly defined in the model. Instead, its impact on foam stability is linked to the concept of limiting water saturation S_w^*, and implicitly to the limiting capillary pressure P_c^* (Khatib et al., 1988), through the relation between water saturation and capillary pressure embodied in the Leverett J-function (Eq. (8)) (Leverett, 1941).

$$r_g = C_g \nabla P^m \tag{4a}$$

$$r_g = C_g \int_{-\nabla P_0}^{-\nabla P_0 + \nabla P} \frac{1}{\sqrt{2\pi}} e^{\left(-\frac{1}{2}t^2\right)} dt = \frac{C_g}{2}\left[\mathrm{erf}\left(\frac{\nabla P - \nabla P_0}{\sqrt{2}}\right) - \mathrm{erf}\left(\frac{-\nabla P_0}{\sqrt{2}}\right)\right] \tag{4b}$$

$$r_c = C_c n_f \left(\frac{1}{S_w - S_w^*}\right)^n \tag{5a}$$

$$r_c = C_c n_f \left(\frac{S_w}{S_w - S_w^*}\right)^n \tag{5b}$$

$$n_{f,LE} = \frac{C_g}{C_c} \nabla P^m \left(S_w - S_w^*\right)^n \tag{6a}$$

$$n_{f,LE} = \frac{C_g}{2C_c}\left[\mathrm{erf}\left(\frac{\nabla P - \nabla P_0}{\sqrt{2}}\right) - \mathrm{erf}\left(\frac{-\nabla P_0}{\sqrt{2}}\right)\right]\left(\frac{S_w - S_w^*}{S_w}\right)^n \tag{6b}$$

$$\lambda_{rg} = \frac{k_{rg}(S_w)}{\mu_g^f} = \frac{k_{rg}(S_w)}{\mu_g^0 + \left(\frac{C_f n_f}{v_g^{\frac{1}{3}}}\right)} \tag{7}$$

$$P_c(S_w) = \sigma_{gw}\sqrt{\frac{\varphi}{k}}\, J(S_w) \tag{8}$$

In these equations, C_g, m, ∇P_0, C_c, n, and S_w^* are model parameters. Details on the parameter definitions in the various models discussed here can be found in the cited references.

Equation (9) is obtained by combining Darcy's law for water and gas at a constant gas fractional flow f_g:

$$\frac{u_w}{u_g} = \text{constant} = \frac{u_t(1-f_g)}{u_t f_g} = \frac{k\,\lambda_{rw}\nabla P}{k\,\lambda_{rg}\nabla P} = \frac{\frac{k_{rw}(S_w)}{\mu_w}\nabla P}{\frac{k_{rg}(S_w)}{\mu_g^0 + \frac{C_f n_{f,LE}}{v_g^{\frac{1}{3}}}}\nabla P} \tag{9}$$

where v_g is gas interstitial velocity, $[f_g\, u_t/(S_g\, \varphi)]$.

The LE bubble density (Eq. (6)) is a function of pressure gradient and water saturation. In these models, pressure gradient is a model input, and the LE solution is analogous to the experimental procedure of a fixed-ΔP experiment. Substituting the definition of bubble density (Eq. (4)) into effective gas viscosity (Eq. (9)) and rearranging yields

$$\frac{(1-f_g)}{f_g} = \frac{\frac{k_{rw}(S_w)}{\mu_w}}{\frac{k_{rg}(S_w)}{\mu_g^0 + \left[\frac{C_f}{v_g^{\frac{1}{3}}}\frac{C_g}{C_c}\left(S_w - S_w^*\right)^n\right]\nabla P^m}} \tag{10a}$$

$$\frac{(1-f_g)}{f_g} = \frac{\frac{k_{rw}(S_w)}{\mu_w}}{\frac{k_{rg}(S_w)}{\mu_g^0 + \left[\frac{C_f}{v_g^{\frac{1}{3}}}\frac{C_g}{2C_c}\left(\frac{S_w - S_w^*}{S_w}\right)^n\right]\left[\mathrm{erf}\left(\frac{\nabla P - \nabla P_0}{\sqrt{2}}\right) - \mathrm{erf}\left(\frac{-\nabla P_0}{\sqrt{2}}\right)\right]}} \tag{10b}$$

For fixed (u_w/u_g), Eq. (10a) or (10b) relates ∇P to v_g, which means it relates ∇P to u_t for given f_g.

We first examine the model of Kam and Rossen (2003). For a given pressure gradient, Eq. (10a) determines a unique combination of equilibrium water saturation and bubble density that satisfies the injected gas fraction f_g. Once water saturation and LE bubble density are determined, the relative mobilities of gas and water as well as the total superficial velocity can be determined. Figs. 2 and 3 illustrate the model's prediction of foam properties as a function of ∇P. The model parameter values employed in these figures are from Kam and Rossen (2003) (Table A1), fit to the data of Gauglitz et al. (2002) in Fig. 1b. Experimental conditions are those noted for Fig. 1b.

Bubble density n_f doesn't increase enough with increasing pressure gradient to reduce gas mobility significantly until pressure gradient reaches a value of about 10^5 Pa/m (Fig. 3a). Upon further increase of pressure gradient, increasing bubble density reduces gas mobility λ_g^f greatly. As gas mobility decreases, water saturation falls to maintain water mobility at its fixed ratio to gas mobility. As a result, total mobility λ_t decreases faster than the increase in ∇P (Fig. 3b). Point B in these figures represents the minimum pressure gradient or velocity that triggers foam generation, ∇P^{gen} or u_t^{gen}. As $[\mathrm{dlog}\,(\lambda_t)/\mathrm{dlog}\,(\nabla P)]$ falls below (-1), u_t decreases with increasing ∇P (Eq. (3)). In the highly non-linear equations of this model, the key factor for triggering foam generation is the power-law dependence of lamella generation upon pressure gradient (Eq. (5a)).

As in Fig. 1b and c, these parameters were fit to data which were taken in experiments under ideal conditions for very strong foam. Therefore the numerical values are not typical of field application under more-challenging conditions, or with supercritical CO_2. This comment applies to the cases discussed below as well. Further work is needed on conditions for foam generation and propagation under less-ideal, more-

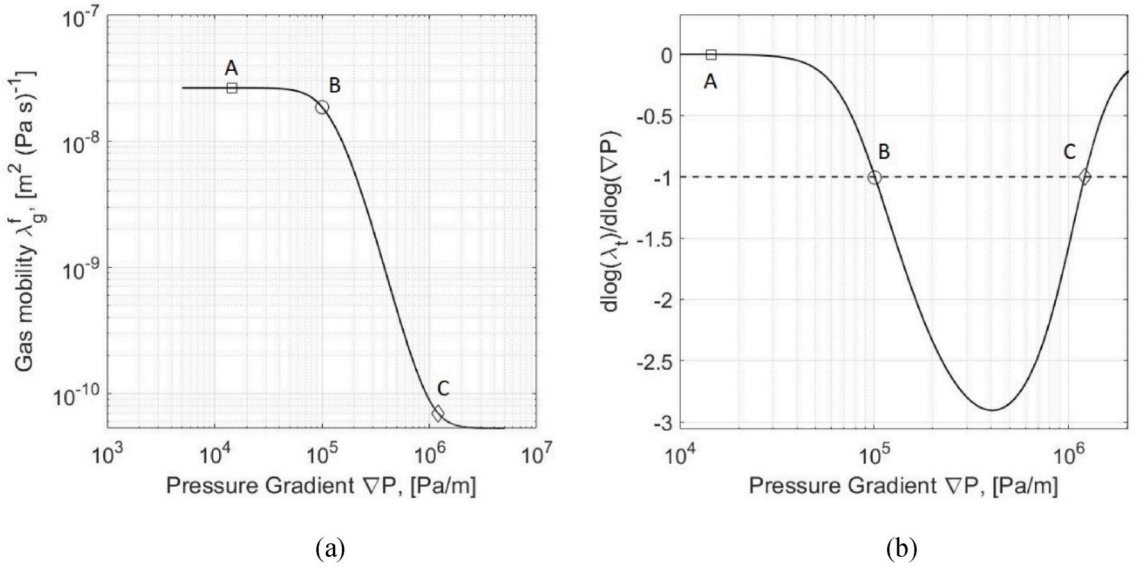

Fig. 3. (a) Mobility of gas with foam ($k \times \lambda_{rg}^f$) as a function of pressure gradient, and (b) [dlog (λ_t)/dlog (∇P)] as a function of pressure gradient for the Population-Balance model of Kam and Rossen (2003). [dlog (λ_t)/dlog (∇P)] < -1 between B and C. This enables the model to represent a trigger for foam generation defined in Eqs. (2) and (3). Parameter values are in Table A1.

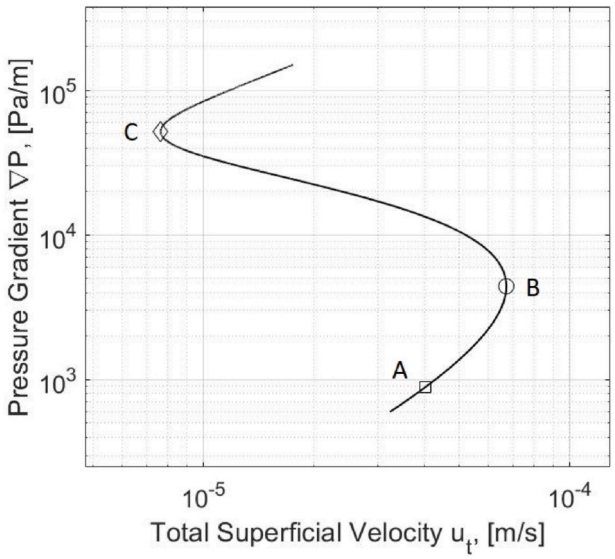

Fig. 4. Local-Equilibrium solution of the Population-Balance model of Kam (2008) at foam quality $f_g = 91\%$. The meanings of A, B and C match those in Figs. 2–4. Parameter values are in Table A2.

realistic field conditions.

2.2. Population-balance model of Kam (2008)

The variant of this model introduced by Kam (2008) employs a modified version of the lamella-creation function r_g: an error function of pressure gradient (Eq. (4b)). In addition, the lamella-coalescence function r_c includes a small modification from Kam et al. (2007) (Eq. (5b)): the lamella-creation rate is constrained between 0 and an upper limiting value. The reference pressure gradient ∇P_0 (Eq. (4b)) indicates the pressure gradient above which the rate of lamella generation starts increasing sharply. Fig. 4 illustrates the LE solution of this model. The model parameters employed in this example are from Kam (2008) (Table A2). The model parameters were evidently fit to data from a beadpack of permeability 30.1 μm^2 (Fig. 9 in Gauglitz et al. (2002)). The surfactant was 2 wt% MA80I (sodium dihexyl sulfosuccinate) in brine of 3 wt% NaCl and 0.01 wt% $CaCl_2$. Fig. 5a and b shows the relation between the reduction of gas mobility and the increase of pressure gradient, which explains the model's representation of a trigger for foam generation specified by Eq. (3).

2.3. Population-balance model of Chen et al. (2010)

The population-balance model of Kovscek and Radke (1993, 1994, 1995) and its variants (e.g. Kovscek and Bertin, 2003; Tang and Kovscek, 2006; Chen et al., 2010) account for an explicit definition of bubble density n_f as well as gas trapping and flowing fraction of gas X_f. In this model, repeated Roof snap-off (Roof, 1970; Ransohoff and Radke, 1988) is the mechanism of lamella generation in steady flow. This mechanism is assumed to operate repeatedly in a fraction of pore throats in steady-state foam flow.

Here we analyse the model of Chen et al. (2010), a version of the model introduced by Kovscek and Radke (1994, 1995). Kovscek and Radke (1993) state that representing a minimum velocity and pressure gradient for foam generation is not a goal of their foam model. They argue that foam generation occurs readily as gas invades a porous medium initially fully saturated with surfactant solution; hence it's unnecessary to include an onset velocity or pressure gradient in the lamella-creation function.

Like other Population-Balance models, the equations in this family of models are nonlinear and complex. We have not been able to reproduce such a trigger with the model parameters we tested. Here we do not attempt to provide a rigorous proof that this family of models cannot reproduce a minimum velocity for foam generation. Instead, we describe conditions under which it could produce a minimum velocity for foam generation.

As in other PB models, in the model of Chen et al. (2010) foam texture n_f is the result of simultaneous processes of lamella creation and destruction. The lamella-generation rate r_g in this model depends on the interstitial velocities of gas and water through generation sites in the pore network:

$$r_g = k_1 v_w v_f^{1/3} \tag{11}$$

where v_w and v_f are the interstitial velocities of water and of flowing gas, respectively, and

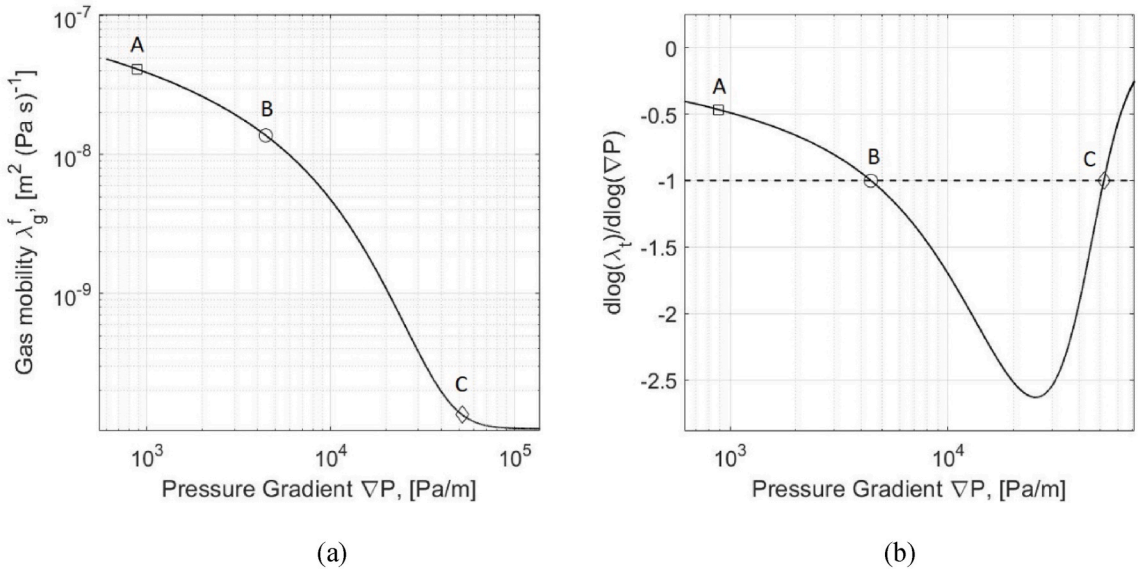

Fig. 5. (a) Mobility of gas λ_g^f as a function of pressure gradient for the Population-Balance model of Kam (2008). (b) [dlog (λ_t)/dlog (∇P)] as a function of pressure gradient. Parameter values are listed in Table A2.

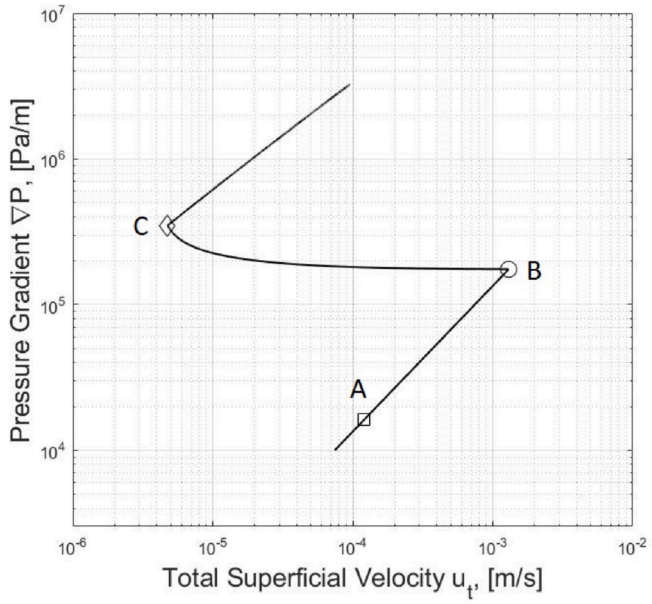

Fig. 6. Local-Equilibrium solution for the Foam Interpolation model in STARS simulator at foam quality of f_g = 90%. Points A, B and C have the same meanings as in Fig. 4–7. Parameter values are in Table A3.

$$k_1 = k_1^0\left[1 - \left(\frac{n_f}{n^*}\right)^{\omega}\right] \tag{12}$$

where n* is the maximum possible foam texture. The term in brackets shuts off foam generation as foam approaches the limiting texture n*. In these and the following equations, k_1^0, ω, n*, $X_{t,max}$, β, k_1^0, and P_c* are model parameters.

The water interstitial velocity v_w is a function of water saturation S_w, porosity φ and water superficial velocity u_w:

$$v_w = \frac{u_w}{\varnothing S_w} \tag{13}$$

The gas interstitial velocity is a function of gas saturation S_g, gas superficial velocity u_f, porosity, and the flowing gas fraction X_f:

$$v_f = \frac{u_f}{\varnothing S_g X_f} \tag{14}$$

The flowing gas fraction in turn depends on foam texture n_f:

$$X_f = 1 - X_{t,max}\left(\frac{\beta n_f}{1+\beta n_f}\right) = \frac{X_{t,max}}{1+\beta n_f} + \left(1 - X_{t,max}\right) \tag{15}$$

where $X_{t,max}$ is the maximum trapped-gas fraction.

In another version of the model (Tang and Kovscek, 2006), the flowing fraction depends on ∇P as well as n_f. In the rest of this derivation we assume the dependency is on n_f alone.

The lamella-destruction rate depends on foam texture, the interstitial velocity of gas through lamella-destruction sites and capillary pressure:

$$r_c = k_{-1} n_f v_f \tag{16}$$

with

$$k_{-1} = k_{-1}^0\left(\frac{P_c}{P_c^* - P_c}\right)^2 \equiv k_{-1}^0\, f(P_c) \tag{17}$$

where k_1^0 is a constant, P_c* is the limiting capillary pressure for foam stability, and we define $f(P_c)$ for convenience in the notation below. Note that $f(P_c)$ increases as P_c increases toward P_c*, where $f(P_c)$ approaches infinity.

Equating the lamella-creation and -destruction rates gives an expression for LE foam texture n_f:

$$n_f = \left(\left[\frac{k_1^0}{k_{-1}^0}\right]\left[\frac{u_w}{u_f}\right]\frac{1^{\frac{1}{3}}}{\varphi}\right)\left[\frac{1-\left(\frac{n_f}{n^*}\right)^{\omega}}{f(P_c(S_w))}\right]\left[\frac{(1-S_w)^{\frac{2}{3}}}{S_w}\right]\left[X_f^{\frac{2}{3}}\right]\left[u_f^{\frac{1}{3}}\right] \tag{18}$$

At a given injected gas fraction, the term in the first bracket is constant. Removing this term, for steady flow at fixed quality one can write

$$n_f \sim \left[\frac{1-\left(\frac{n_f}{n^*}\right)^{\omega}}{f(P_c(S_w))}\right]\left[\frac{(1-S_w)^{\frac{2}{3}}}{S_w}\right]\left[X_f^{\frac{2}{3}}\right]\left[u_f^{\frac{1}{3}}\right] \tag{19}$$

At a trigger for foam generation at fixed foam quality, as ∇P increases, total superficial velocity u_t decreases (Fig. 1b), n_f increases, S_w decreases, and P_c increases. This trend continues as ∇P increases through the intermediate unstable state of foam, while foam texture

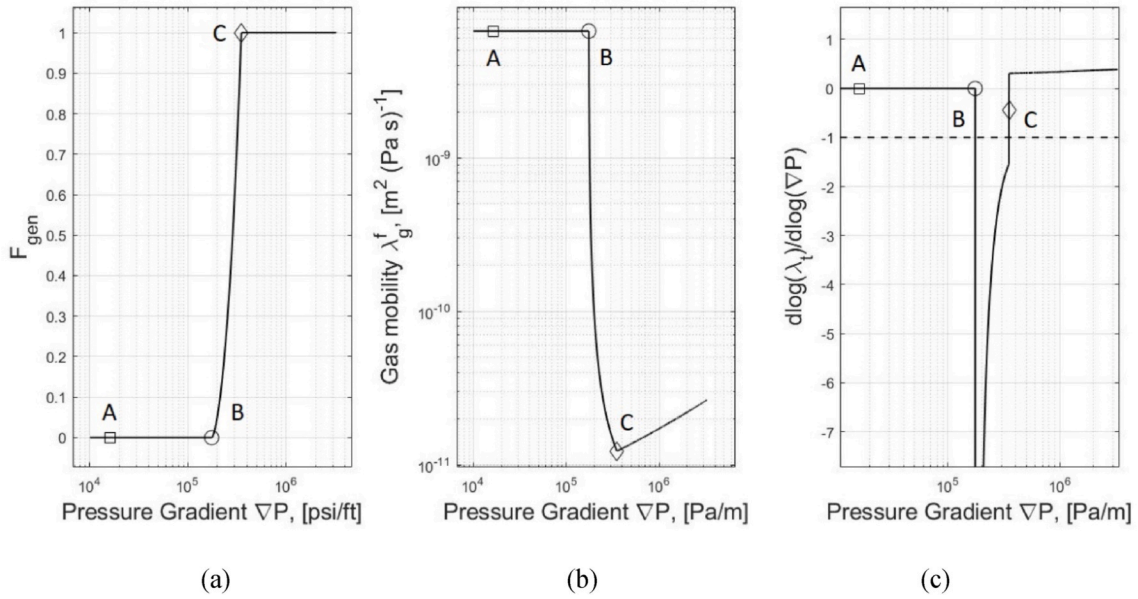

Fig. 7. (a) Foam-generation factor F_{gen} as a function of pressure gradient for the Foam Interpolation model in STARS simulator at foam quality of $f_g = 90\%$. (b) Gas mobility λ_g^f as a function of pressure gradient ∇P. (c) [dlog (λ_t)/dlog (∇P)] as function of pressure gradient. Parameter values are in Table A3.

rises from nearly zero to near its maximum value, flowing fraction falls from a value close to 1 toward its minimum value, water saturation falls from a value near (1-S_{gr}) to a value near S_{wc}. The initial triggering of foam generation occurs at a relatively large value of S_w, given the high mobility of gas in the absence of foam.

Based on Eq. (19), consider how n_f could increase as u_t decreases. The individual terms in Eq. (19) affect n_f as follows:

1) The first term in brackets decreases as f(P_c) increases with increasing P_c.
2) The third term in brackets decreases as foam texture n_f increases (Eq. (15)). In the model of Tang and Kovscek (2006), where flowing fraction depends also on foam ∇P, flowing fraction is an increasing function of ∇P. Thus in that version of the model, the superficial velocity of flowing foam would likewise fall as flowing fraction increases.
3) The fourth term in brackets decreases as total superficial velocity decreases at fixed gas fraction.
4) The second term in brackets is the only term that increases as foam is generated and water saturation falls. This term derives from the dependence of gas and water interstitial velocities through generation sites (Eq. (11)) and the relations between interstitial and superficial velocities of water and gas (Eq. (13)) and (Eq. (14)).

Therefore, an increase in foam texture upon a reduction in superficial velocity is in principle possible if the increase in the second term is larger than the decreases in the first, third and fourth terms.

The extent to which water saturation falls as foam is created depends on the mobility functions for gas and water. The mobility of water depends on the water-relative-permeability function. The mobility of gas depends on the foam-free gas relative-permeability function and foam texture:

$$\lambda_{rg} = \frac{k_{rg}^f}{\mu^f} = k_{rg}(S_w)\left(\mu_g^0\left[1 + \frac{\alpha}{\mu_g^0} * \frac{n_f}{v_g^{\frac{1}{3}}}\right]\right)^{-1} \tag{20}$$

where k_{rg}^f and k_{rg} are the gas relative permeabilities as a functions of S_w with and without foam, μ_g^f and μ_g^0 are gas viscosity with and without foam, and α is a parameter in the gas-viscosity model. The decrease in gas mobility, which causes the fall in water saturation, is tempered by the shear-thinning rheology of foam and the effect of decreasing water saturation on foam-free gas relative permeability. At the trigger itself, X_f is close to 1, and hence that term is unlikely to reduce gas mobility greatly (by reducing the gas phase relative permeability).

2.4. STARS Foam Interpolation model

The Foam Interpolation model in the STARS simulator (Martinsen and Vassenden, 1999; Cheng et al., 2000; Computer Modeling Group, 2017) is a widely used Implicit-Texture foam model. Lotfollahi et al. (2017) state that the STARS model cannot represent the hysteresis seen in foam-generation experiments. It is not clear if they mean the abrupt change of state upon foam generation, or hysteresis in strong foam when injection rate is reduced.

In the STARS model, the effect of foam on gas mobility is represented as a reduction in gas relative permeability in the presence of foam. The relative permeability of gas is the product of gas relative permeability without foam, k_{rg}, and a mobility-reduction factor FM (Eq. (21)). FM is in turn a function of seven factors representing the effects of pressure gradient, water and oil saturations, surfactant concentration, etc. (Ma et al., 2013). Parameter fmmob (Eqs. (21) and (22)) is the reference gas-mobility-reduction factor, which represents the maximum achievable reduction in gas mobility. In the following equations, fmmob, fmgcp, epgcp, epdry, fmdry, fmcap and epcap are model parameters. Parameters fmdry and epdry were recently renamed sfdry and sfbet in the simulator (Computer Modeling Group, 2017).

$$\lambda_{rg} = \frac{k_{rg(S_w)}}{\mu_g} FM \tag{21a}$$

$$FM \equiv \frac{1}{1 + fmmob \times \prod_{i=1}^{7} F_i} \tag{21b}$$

Here we examine three F_i functions from Eq. (21) to represent the model's ability to represent a trigger for foam generation in an oil-free homogeneous porous medium:

1) The foam-generation function (Eq. (24)), called F_{gen} by Lotfollahi et al. (2017) and F_4 by Ma et al. (2015), is a function of capillary number N_{ca}, which is defined in terms of pressure gradient ∇P (Eq. (23)).

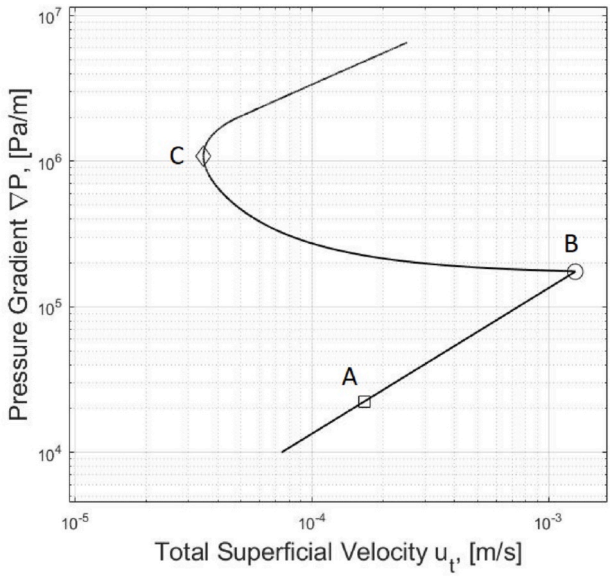

Fig. 8. Local-Equilibrium solution for the foam model of Lotfollahi et al. (2017), a modification of the STARS model, at foam quality $f_g = 90\%$. Parameter values are in Table A4.

2) The dry-out function (Eq. (25)) F_{dry} (also called F_7) is a function that relates water saturation to the reduction of gas-phase mobility by foam. As in the coalescence function in the models of Kam and Rossen (2003), it implicitly reflects the limiting capillary pressure.
3) The shear-thinning function (Eq. (26)) F_{shear} (Lotfollahi et al., 2017) (also called F_3) is also a function of capillary number N_{ca} (Eq. (13)). It accounts for the shear-thinning rheology of strong foam. F_3 equals unity when capillary number is smaller than a reference capillary number fmcap (Eq. (26)).

$$FM = \frac{1}{1 + fmmob\ F_{gen}F_{dry}F_{shear}} \tag{22}$$

$$N_{ca} \equiv \frac{k|\nabla P|}{\sigma} \tag{23}$$

$$F_{gen} = \begin{cases} 0, & N_{ca} \le fmgcp \\ \left(\dfrac{N_{ca} - fmgcp}{fmgcp}\right)^{epgcp}, & N_{ca} > fmgcp \\ 1, & Nca\ >\ 2\ fmgcp \end{cases} \tag{24}$$

$$F_{dry} = 0.5 + \frac{1}{\pi}\arctan(sfbet(S_w - sfdry)) \tag{25}$$

$$F_{shear} = \begin{cases} 1, & N_{ca} \le fmcap \\ \left(\dfrac{fmcap}{N_{ca}}\right)^{epcap}, & N_{ca} > fmcap \end{cases} \tag{26}$$

$$\lambda_{rg} = \frac{k_{rg}(S_w)}{\mu_g}\ \frac{1}{1 + fmmob\ F_{gen}F_{dry}F_{shear}}, \tag{27}$$

$$\frac{u_w}{u_g} = constant = \frac{(1 - f_g)}{f_g} = \frac{\frac{k_{rw}(S_w)}{\mu_w}}{\frac{k_{rg}(S_w)}{\mu_g}\ \frac{1}{1+fmmob\ F_{gen}(\nabla P)F_{dry}F_{shear}}}, \tag{28}$$

The function F_{gen} plays the key role in the model's representation of a trigger for foam generation. This function employs a threshold capillary number fmgcp. In Eq. (23), permeability k and surface tension between gas and water (with surfactant) σ are constants in an isothermal and homogeneous system. Therefore foam generation is a function of pressure gradient. If $\nabla P < (fmgcp \times \sigma/k)$, $F_{gen} = 0.0$ and $FM = 1.0$: no foam exists. As ∇P exceeds this value, F_{gen} increases with increasing ∇P until it reaches unity at [2 (fmgcp)]. Parameter epgcp (Eq. (24)) is an exponent that dictates how F_{gen} increases with increasing ∇P.

The definition of F_{gen} (Eq. (24)) makes gas mobility a function of pressure gradient in a similar way to the effect of the lamella-creation function r_g (Eq. (4a)) and (Eq. (4b)) of the population-balance model of Kam and Rossen (2003). However, in contrast to PB models, the STARS foam model doesn't account explicitly for the dynamics of lamella transport, creation and destruction.

Figs. 6 and 7 show the behavior of the STARS model using parameter values fit by Lotfollahi et al. (2016) to data of Gauglitz et al. (2002) shown in Fig. 1b. As in the model of Kam and Rossen (2003) and its variants (Kam et al., 2007; Kam, 2008), foam generation is triggered by increasing pressure gradient, causing an abrupt decrease in gas mobility with increasing ∇p. Weak foam (between points A and B) in Figs. 2–5 in those models refers to a state where some lamellae exist but have relatively little effect on gas mobility. In the Foam Interpolation model of STARS, however, there is no foam (no mobility reduction) for $\nabla P < (fmgcp \times \sigma/k)$ (Eq. (24)).

2.5. *Lotfollahi et al. (2017) model*

Lotfollahi et al. (2017) focus not on an abrupt change from weak/no foam to strong foam but on hysteresis in foam strength in strong foam: specifically, in the strong-foam state, ∇P decreasing but a small amount upon a reduction in superficial velocity. They propose a new formulation for the foam-generation function F_{gen} in STARS (24), which we denote F^L_{gen} (29):

$$F^L_{gen} = \begin{cases} 0, & N_{ca} < fmgcp \\ fgenc + \left[\dfrac{(1 - fgenc)N^{epgcp}}{1 + N^{epgcp}}\right], & fmgcp \le N_{ca} < N^{max}_{ca} \\ 1, & N^{max}_{ca} \le N_{ca} \end{cases} \tag{29}$$

with N_{ca} defined by Eq. (23) and

$$N \equiv (N_{ca} - fmgcp) \,/\, \left(N^{max}_{ca} - N_{ca}\right). \tag{30}$$

Apart from examining hysteresis in the strong-foam state, Lotfollahi et al. (2017) show that the new function can be used to predict a minimum velocity (and minimum pressure gradient) for foam generation. In the revised function, a maximum capillary number N^{max}_{ca} (related to a maximum pressure gradient ∇P^{max}) is introduced in addition to the minimum capillary number for foam generation fmgcp. The foam-generation function F^L_{gen} is a power-law function of a normalized capillary number N (30). For $N_{ca} < fmgcp$, $F^L_{gen} = 0.0$: gas and water flow in the absence of foam. For $N^{min}_{ca} \le N_{ca} < N^{max}_{ca}$, foam generation is triggered and F^L_{gen} increases with increasing pressure gradient. For $N_{ca} \ge N^{max}_{ca}$, $F^L_{gen} = 1.0$, indicating the steady state of strong foam is achieved. The difference between N^{min}_{ca} and N^{max}_{ca} governs the range of the steady state of intermediate foam. Figs. 8 and 9 show model behavior using parameter values fitted by Lotfollahi et al. (2017) to the data in Fig. 1b (and Table A4).

In analysing the Lotfollahi et al. foam model, we employ the same combination of FM functions shown in Eq. (22) and the updated foam-generation function (Eq. (24)), the dry-out function F_{dry} (Eq. (25)), and the shear-thinning function F_{shear} (Eq. (26)). Fig. 9b shows the impact of increasing pressure gradient on gas mobility as well as the magnitude of reduction of gas mobility. As pressure gradient exceeds the minimum pressure gradient for foam generation, FM decreases sharply, which brings about a significant reduction of gas mobility λ^f_g. Fig. 9c illustrates the range of pressure gradient where $[d\log(\lambda_t)/d\log(\nabla P)] < (-1)$, within which total superficial velocity decreases with increasing ∇P. The foam model of Lotfollahi et al. (2017) can represent a trigger for foam generation.

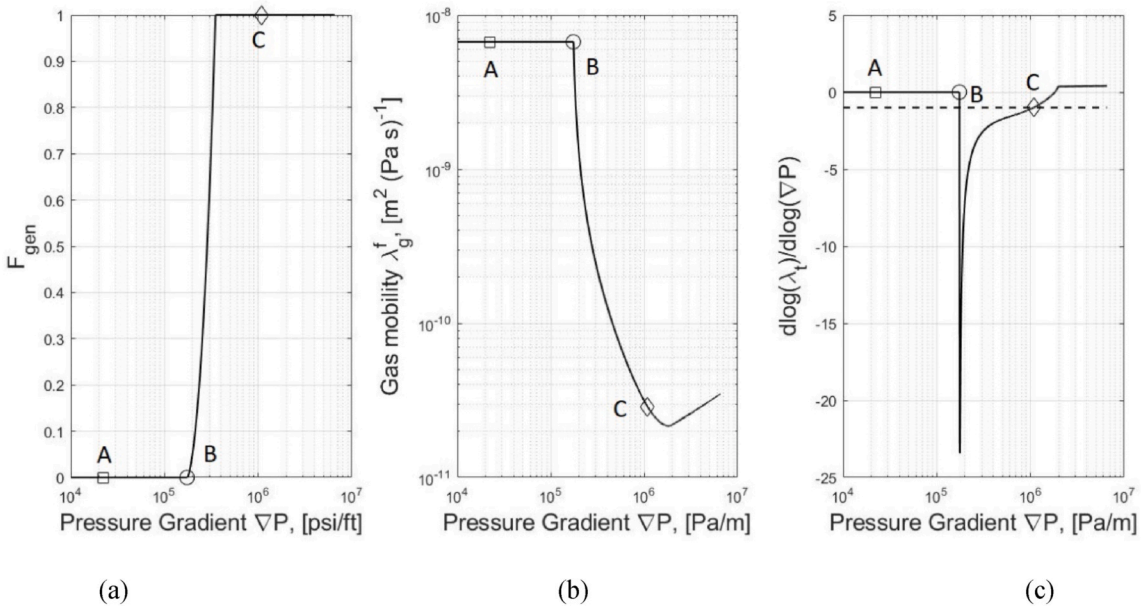

Fig. 9. (a) Foam-generation function F_{gen}^{L} (Eq. (19)) as function of pressure gradient ∇P or the foam model of Lotfollahi et al. (2017). (b) Gas mobility (with foam) as a function of pressure gradient ∇P. (c) [dlog (λ_t)/dlog (∇P)] as a function of pressure gradient. Parameter values are in Table A4.

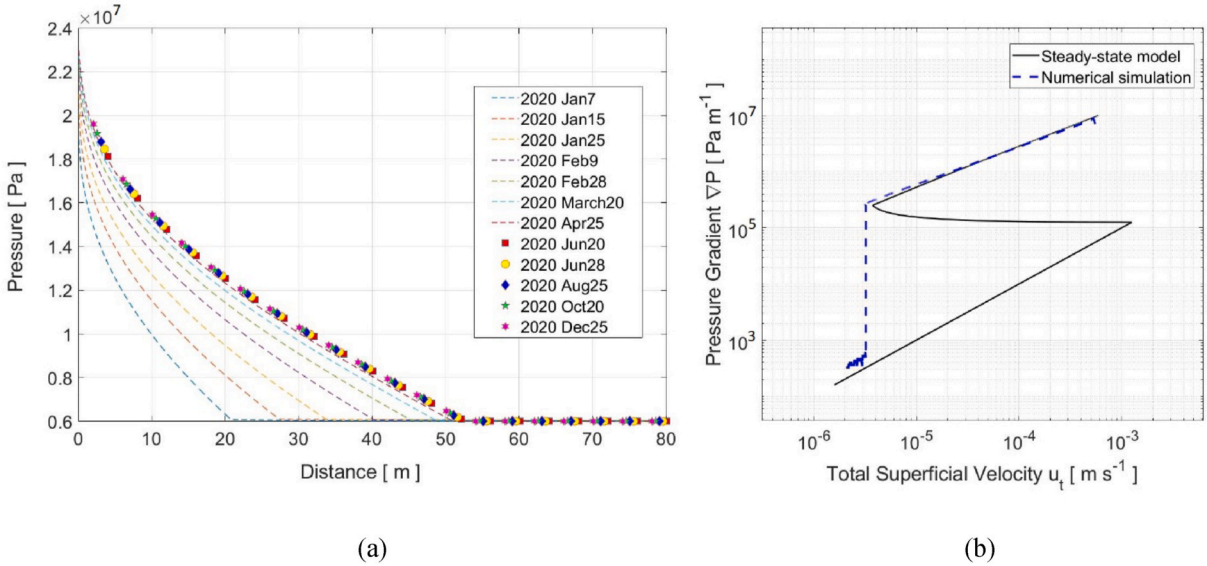

Fig. 10. (a) Reservoir pressure distribution around injection well as a function of time. Plots from June 20 through Dec. 25 overlap here. (b) Grid-block values of pressure gradient and superficial velocity (blue dashed curve) at the end of the simulation. The data would be the same for any date from June 20 onward. The black curve is the local-equilibrium behavior predicted by STARS (cf. Fig. 6). By this time the rise in pressure at the well and gas compressibility reduce superficial velocity there below the threshold velocity for foam generation. When injection began, at the initial reservoir pressure, foam generation was initiated at a velocity greater than the threshold velocity. (For interpretation of the references to colour in this figure legend, the reader is referred to the Web version of this article.)

3. Simulation of foam generation and propagation

Since the STARS foam model includes the effect of a minimum superficial velocity for foam generation (Fig. 6), we investigate how this model represents foam generation and propagation in radial flow. Ashoori et al. (2012) and Yu et al. (2020) find that the velocity of the foam front decreases and approaches zero at a finite total superficial velocity u_t^{prop}. This threshold velocity for foam propagation is greater than that at which strong foam cannot be maintained in place, u_t^{col} (Fig. 1c). We examine whether or not the simulation result from the IT foam model STARS can match this result.

3.1. Model description

We assume a one-dimensional horizontal cylindrical reservoir with homogeneous permeability (10 Darcy) and porosity ($\varphi = 0.199$), and an outer radius of 80 m. The simulation uses a 36° radial arc, but the superficial velocities cited below are scaled to injection in the full radial direction. The model has 8000 grid blocks of length 0.01 m in the radial direction. Gas and surfactant solution are co-injected from an injection well of radius 0.1 m.

The reservoir is initially fully saturated with brine without surfactant. We start the simulation by co-injecting gas and brine solution for around 9 days, when a quasi-steady state between gas and water is

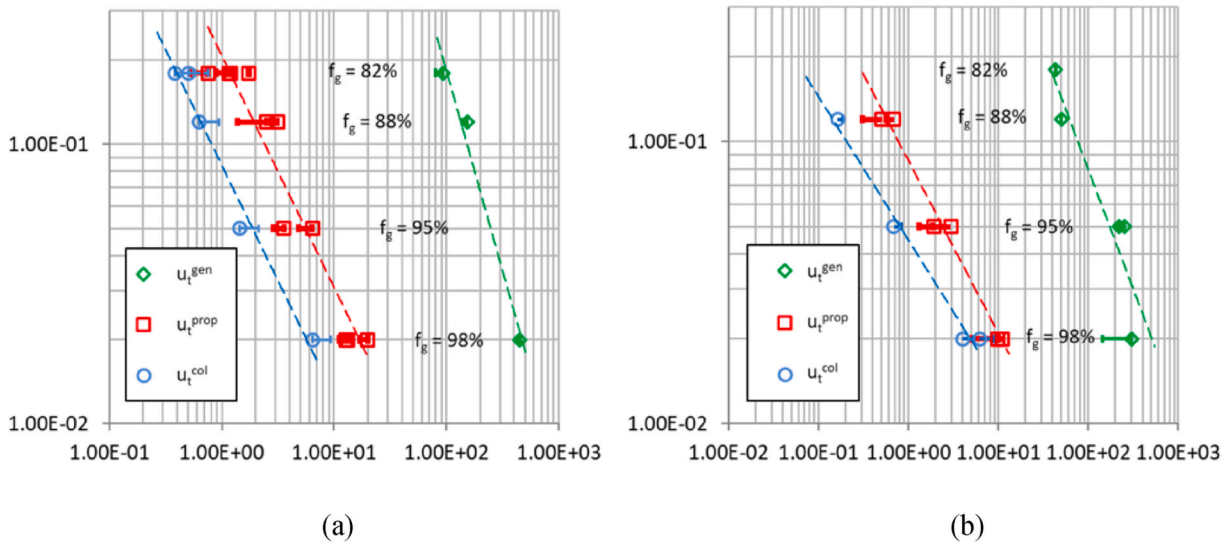

Fig. 11. Critical superficial velocities (horizontal axis, ft/day) for generation, propagation, and destruction of foam, from Yu et al. (2020). Vertical axis is foam quality. (a) Experimental data for surfactant concentration of 0.05 wt%. (b) Experimental data for surfactant concentration 0.3 wt%. Error bars are difference between velocities at last data point before transition and past transition.

achieved in the first half of the reservoir, which extends to an outer radius of 80 m. We then switch to the co-injection of gas and surfactant solution.

The initial reservoir pressure is 6000 kPa, and the outer radius is maintained at a minimum bottom-hole pressure of 5990 kPa. The initial and injection temperatures (27°C) are far below the bubble point of water (275 K) at this pressure. The relative-permeability tables for gas and water phases are based on Brooks-Corey expressions (Table A3), with parameters taken from Lotfollahi et al. (2017). Rock and fluid properties used in our simulation are also given in Table A3.

3.2. Simulation result

Co-injection of N_2 gas and surfactant solution starts on Jan 1 and stops on Dec 31. The total volumetric injection rates of gas and liquid are fixed at surface conditions corresponding to a foam quality of 90% at the initial reservoir pressure. This indicates an initial total superficial velocity of about 1.67×10^{-3} m/s in at the injection well. This injection rate guarantees that the initial total superficial velocity u_t at the boundary of the first grid block is greater than the minimum superficial velocity for foam generation u_t^{gen} based on the LE equations (Fig. 6). As a result, the pressure gradient and capillary number inside the first grid block (as well as the blocks nearby) are high enough to satisfy the criterion (Eq. (24)) for foam generation. Later, pressure rises greatly near the well (Fig. 10a) and results in gas compression and a reduction of gas injection rate. However, since foam propagation is determined at the leading edge of the foam bank, which remains near the initial reservoir pressure, this does not affect foam propagation.

Fig. 10a illustrates the evolution of reservoir pressure during foam injection. The pressure profiles from Jan 7 to Jun 20 indicate the propagation of foam to greater distances. Foam propagation stops by June 20 at a distance of about 52 m from the well. The leading edge of foam bank remains there for another 6 months of foam injection.

In the STARS simulation, the failure of foam propagation is directly related to the inability to maintain foam, not to a separate condition for foam propagation. Fig. 10b compares the result of numerical simulation (blue dashed-curve) of foam generation and subsequent propagation to the solution of the local-steady-state model (black solid curve). The numerical simulation result (blue curve in Fig. 10b) represents the grid-block superficial velocities and pressure gradients on Dec 25, one year after the start of foam injection. Upon achieving quasi-steady state (on June 20), the pressure at the well grid block has increased significantly over the initial reservoir pressure (Fig. 10a). Due to gas compressibility, total superficial velocity near the injection well has fallen from that when foam generation was triggered. Nevertheless, the numerical simulation result is still in good agreement with the local-equilibrium solution of the model for the nominal gas fractional flow (Fig. 10b).

In this radial simulation with tiny grid blocks, we avoid another, more-fundamental problem in representing foam generation near an injection well in reservoir-scale simulation. The Peaceman (1978) equation, used in simulations with non-radial grids, represents injection-well pressure based on averaged fluid properties in the grid block containing the injection well. If fluid properties depend on pressure gradient, in the simulation they are based on estimated pressure difference between the well grid block and its neighbouring grid blocks instead of at the wellbore. Injection/production wells are modelled as a source/sink term in governing equations. As a result, the pressure gradient at the wellbore is not calculated explicitly in a conventional reservoir simulation. In Fig. 10b foam generation reflects the pressure difference between the first and second grid blocks (V. Chandrasekar, Computer Modeling Group, personal communication): in our simulation, at a position 1 cm from the wellbore (or equivalently 11 cm from the centre of injection well).

In a simulation of the same radial reservoir using grid blocks 0.1 m long, foam generation fails. There is no foam generation in this case, because superficial velocity (about 9.2×10^{-4} m/s) and pressure gradient at the outer surface of the first grid block (radius 20 cm) is not sufficient for the triggering of foam generation. In a conventional reservoir simulation the distance from the well to the grid-block boundary would usually be much greater. Pressure gradient as calculated between grid blocks in the simulation would not reflect wellbore pressure gradient or foam generation at the wellbore.

This issue would affect not only the STARS model, but that of Lotfollahi at al. (2017) and the Population-Balance model of Kam and Rossen (2003) and its variants (Kam et al., 2007; Kam, 2008). Unless grid resolution gives a superficial velocity at the grid-block scale sufficient for foam generation, the models would not indicate that foam generation occurs. Population-Balance models have the option of injecting gas with a non-zero value of n_f reflecting the presence of foam; this foam would presumably be maintained in propagation to other grid blocks. But this then reflects a choice of the properties of injected gas made manually by the user, not a triggering of foam generation in situ at

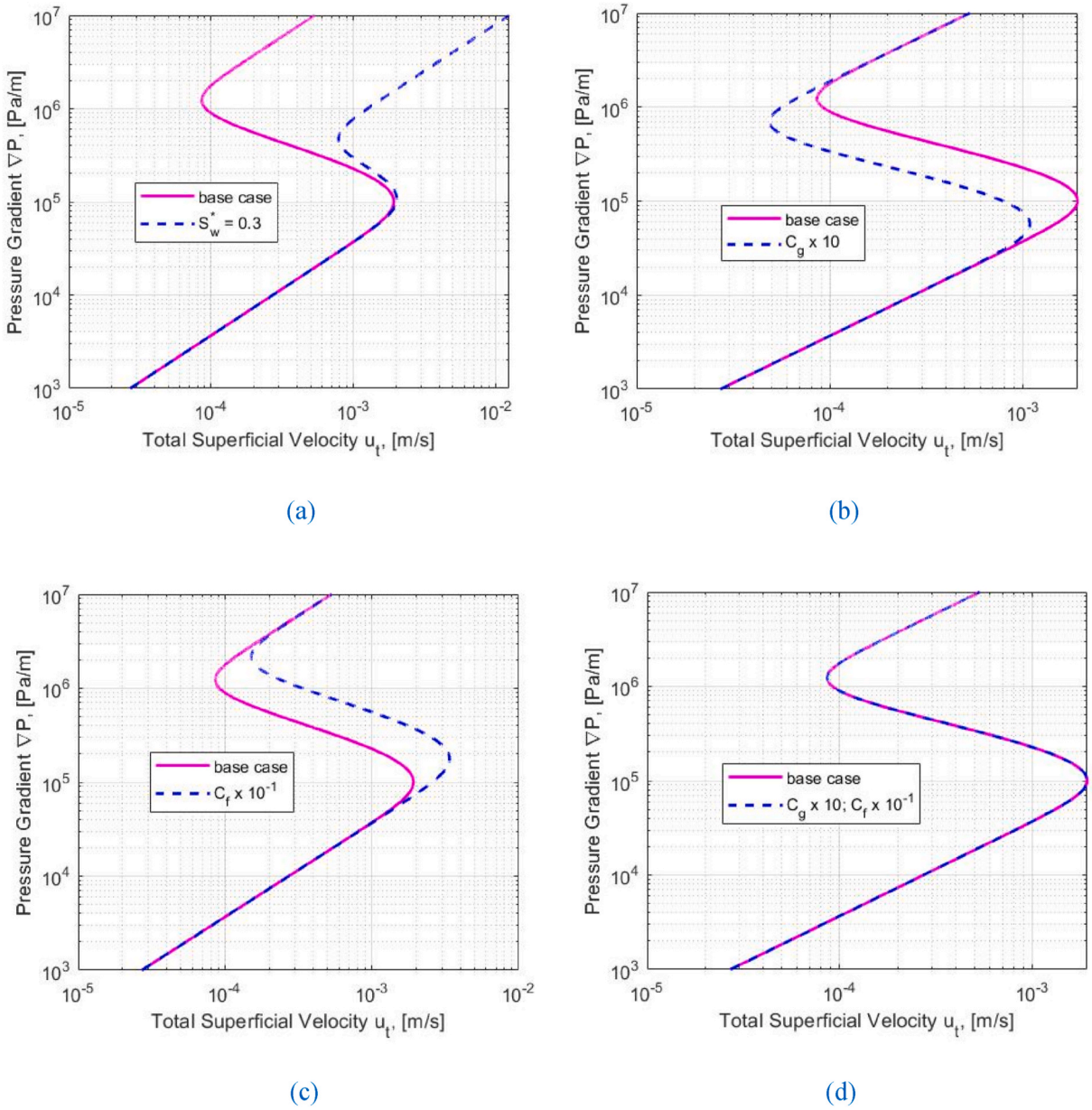

Fig. 12. The effects on the model of Kam and Rossen of (a) increasing S_w* from 0.22 to 0.3; (b) increasing C_g by a factor of 10; (c) reducing C_f by a factor of 10; (d) both increased C_g and reduced C_f, since both effects would be expected upon a reduction in surface tension. Foam quality $f_g = 0.9$ in all four cases. The base-case values of model parameters are given in Table A1.

the injection face. If the user makes this choice, there would be foam entering the grid block whether or not ∇P at the injection face were sufficient to trigger foam generation.

Simulations of foam in linear flow (Kam et al., 2007; Kam, 2008; Lotfollahi et al., 2017) with these models provide valuable insights into foam mechanisms. They avoid the issue described in the previous paragraph, because total superficial velocity is uniform in the linear model (apart from possible effects of the compressibility of gas). This issue would arise, however, in reservoir application of the model with injection wells located inside a relatively large grid block.

Lee et al. (2016) analyse foam propagation using a variant of the PB model of Kam (2008). They analyse the local-equilibrium behavior of the foam model, and determine foam behavior as a function of injection rate, foam quality and radial distance from the well. Specifically, they assume strong foam is generated at the well based on superficial velocity there, and then determine the radial distance where strong foam collapses and propagates no further. Because they apply the LE version of the model, foam propagation fails where $u_t = u_t^{col}$, not at a separate u_t^{prop}. Izadi and Kam (2019) apply a similar technique to analyse the effects of injected foam quality and nature of the gas phase and discuss how to fit model parameters and a comparison to the effects of gravity segregation. Izadi et al. (2021) used the LE behavior of the PB foam model to define a single approximate value of the mobility-reduction factor to apply in the STARS model to simulate foam application for each of several cases designed to represent field applications. These studies do not implement the PB foam model directly in numerical simulation.

IT foam models do not track foam propagation directly. Foam is created in the next grid block at the foam front when the estimated pressure gradient in that grid block exceeds ∇P^{min} (Eqs. (24) and (29)). Pressure gradient in that grid block is inferred from the pressures in grid blocks upstream and downstream of it. Therefore, with no foam in the given grid block or that ahead of it, the creation of foam in the grid block at the foam front requires a large-enough pressure in the upstream grid block that the pressure gradient calculated for the grid block at the front

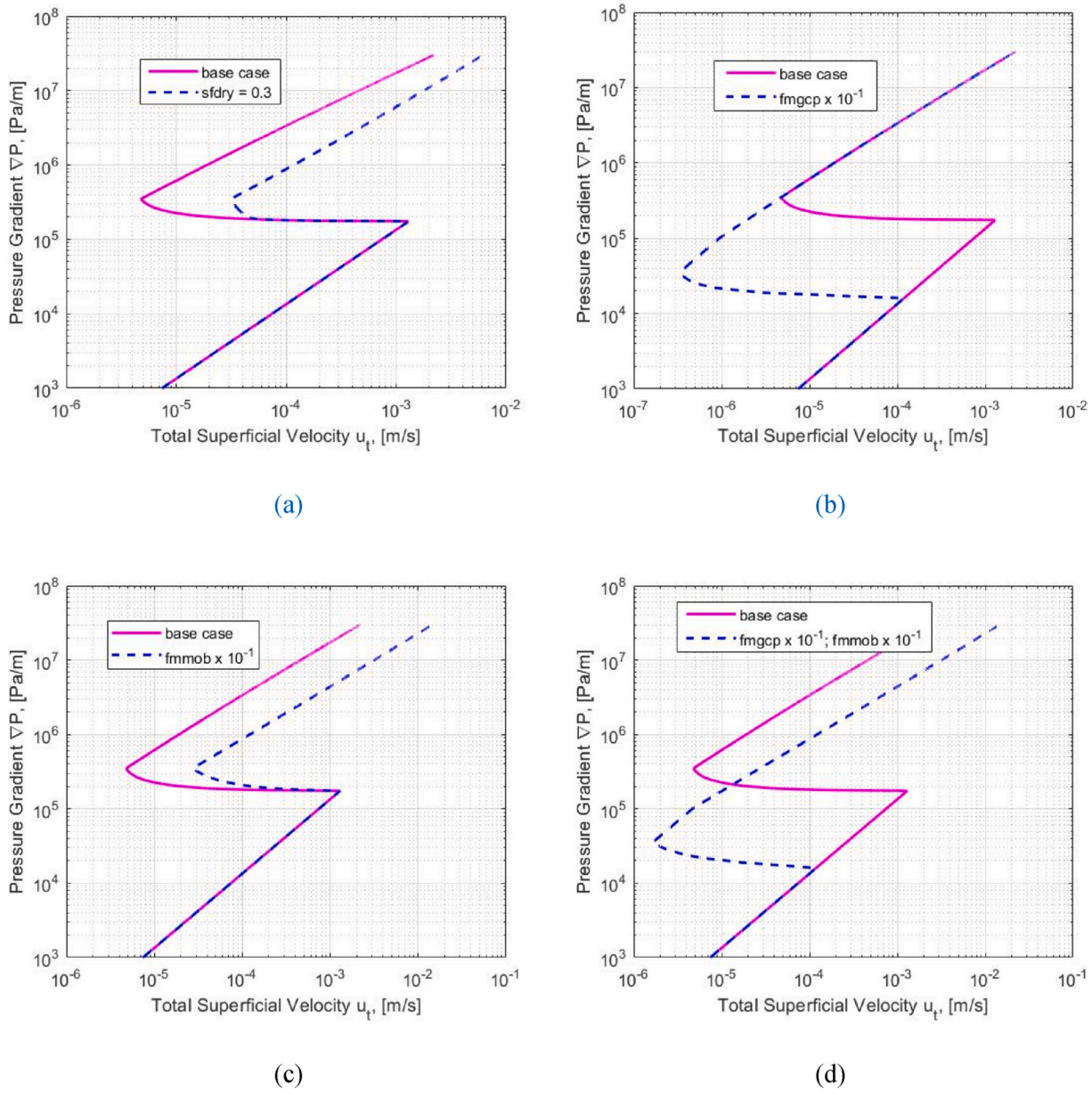

Fig. 13. The effects on the STARS model of (a) increasing sfdry (fmdry) from 0.22 to 0.3; (b) reducing fmgcp by a factor of 10; (c) reducing fmmob by a factor of 10; (d) reducing both fmgcp and fmmob by a factor of 10. Foam quality $f_g = 0.9$ in all four cases. The base-case values of model parameters are given in Table A3.

exceeds ∇P^{min}. For PB models gas enters the grid block with the foam texture of the upstream grid block and this is not a limitation.

If foam generation is achieved, foam propagation depends on the pressure gradient assigned to the grid block at the foam front. The STARS simulator uses the Euclidian average of the pressure differences upstream and downstream of that grid block (V. Chandrasekar, Computer Modeling Group, personal communication). This heavily weights the large upstream pressure difference, giving successful foam propagation in our simulations. If an arithmetic average were used, foam propagation would be expected to fail when the pressure gradient, based on the difference in pressure between the grid block at the front and that upstream, is roughly twice that required for foam propagation.

Two additional implications present themselves: First, if surfactant and gas are both present, and foam generation results in one grid block, in each subsequent time step foam could advance to the next grid block. The advance of the foam state could be nearly instantaneous, faster than foam bubbles themselves could advance. Second, this criterion does not depend on whether the strong foam is present in the upstream or the downstream grid block. This numerical algorithm could produce backwards foam propagation as seen in a number of laboratory studies (e.g. Apaydin and Kovscek, 2001; Simjoo et al., 2012). The backwards growth of the foam front would be very rapid, whereas that seen in the laboratory in these cases is slow.

4. Model implications for field applications of foam

As noted, the model results shown above are mostly based on parameter fits to experiments conducted under ideal conditions for strong foam. The minimum velocity and pressure gradient for foam generation are substantial in these examples, and the pressure gradient for foam propagation is impractically large for field application. The minimum velocity for generation itself is not a significant issue for field application; velocities are very large at the injection well. The pressure gradient near the injection well *is* a serious issue for co-injection: fracturing of the well can result (Kuehne et al., 1990; Martinsen and Vassenden, 1999; Blaker et al., 2002). However, most foam field

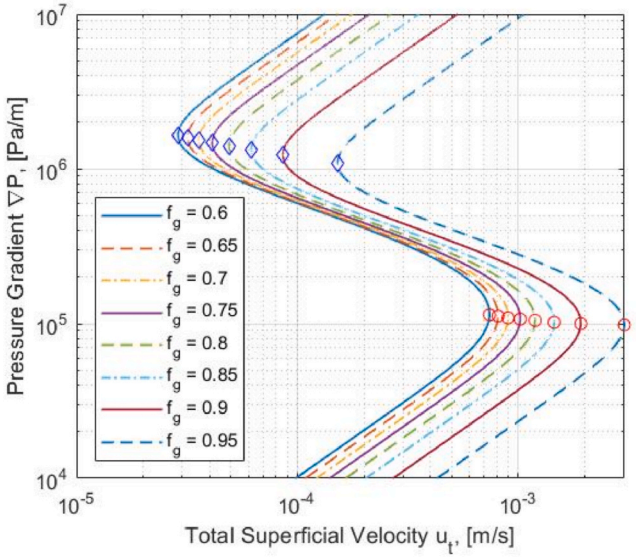

Fig. 14. Steady-state total superficial velocity as a function of pressure gradient for given foam qualities f_g, from the population balance model of Kam and Rossen (2003) for one set of model parameters (Table A1).

applications use SAG injection, where foam generation is much easier and injectivity greater. Even for SAG foam injection, possible limits to foam propagation are important, however. If slugs are relatively small, conditions at the foam front approximate constant quality (Stone, 1982).

There are a wide range of differences between the experiments behind our figures and field applications of foam. Unfortunately, datasets like Fig. 1b and c for fitting models for foam generation are rare. Lotfollahi et al. (2016) fit the model of Kam (2008) to supercritical CO_2 foam data of Moradi-Araghi et al. (1997) and N_2 foam data of Alvarez et al. (2001). Their focus was on fitting steady-state strong-foam behavior as a function of foam quality at fixed velocity, not on foam generation. There were no data for foam generation from these studies, and Lotfollahi et al. used a near-zero pressure gradient for foam generation, $\nabla P_o = 226$ Pa m^{-1} (0.01 psi ft^{-1}), for both cases in their fit. Yu et al. (2020) plot how the critical velocities for N_2 generation, propagation and stability vary with surfactant concentration and foam quality in their experiments (Fig. 11).

In the absence of a range of datasets at different conditions, here we consider how models might adapt to two differences in behavior. First, conditions in the field are often much more problematic for foam stability: higher temperature and salinity, less-water-wet rock, presence of residual oil, etc. Second, supercritical CO_2 has much lower surface tension than N_2 against surfactant solution. This suggests less capillary resistance to flow and less gas trapping by capillary forces, resulting in foam generation at much lower pressure gradient (Gauglitz et al. (2002)) and greater foam mobility.

Here we illustrate simple adjustments of model parameters to reflect these differences for two models discussed in the paper: the population-balance model of Kam and Rossen (2003), and the STARS foam model. Reduced foam stability would be reflected by a larger value of S_w^* or fmdry (called sfdry in current version of STARS simulator), respectively, in the two models. Easier mobilization (easier foam generation and greater mobility of strong foam) would be reflected in larger values of C_g and smaller value of C_f for the model of Kam and Rossen (2003), and reduced values of fmgcp and fmmob for STARS.

Fig. 12 shows the effect of these parameter adjustments for the model of Kam and Rossen. A less-stable foam (Fig. 12a) has the same threshold velocity and ∇P for foam generation but lower ∇P for strong foam, and foam collapse at a larger velocity, though smaller ∇P. Parameters C_g and C_f have opposing effects. Larger C_g (easier foam generation) gives generation at a lower velocity and ∇P, and maintenance of strong foam to lower velocity and ∇P (Fig. 12b). Smaller C_f has the reverse effect (Fig. 12c). If the adjustments in the two parameters is inversely proportional (Fig. 12d) the effects cancel out (Eqs. (10a) and (10b)). Of course although both parameters would be expected to change with lower surface tension and easier mobilization, there is no reason why the effects should be exactly inversely proportional as in Fig. 12d.

Fig. 13 shows the effect of parameter adjustments for the STARS model. As in Fig. 12, less-stable foam (Fig. 13a) has the same threshold for foam generation but lower ∇P for strong foam, and foam collapse at a larger velocity, though smaller ∇P. Smaller fmgcp (easier foam generation) gives generation at a lower velocity and ∇P, and maintenance of strong foam to lower velocity and ∇P (Fig. 13b). Smaller fmmob has no effect on generation but gives a lower ∇P for strong foam (Fig. 13c). If fmgcp and fmmob are both reduced (Fig. 13d), threshold velocities and ∇P for generation and maintenance are reduced, and ∇P is reduced for strong foam.

The model of Rossen and Gauglitz (1990) indicates that foam generation requires somewhat smaller ∇P at lower foam quality. None of the models in this study incorporate this dependence, which would imply that C_g or fmgcp depend on f_g. Fig. 14 shows the effect of foam quality on the multiple steady states predicted by the Kam and Rossen model (Kam and Rossen, 2003) for one set of model parameters (Table A1).

5. Conclusions and discussion

The PB models of Kam and Rossen (2003) and Kam (2008), the IT STARS foam model (Computer Modeling Group, 2017), and that of Lotfollahi et al. (2017) can represent a minimum superficial velocity or pressure gradient for foam generation. In steady flow at constant foam quality f_g, if the reduction in gas mobility with increasing ∇P is greater than the increase in ∇P, then total superficial velocity decreases with increasing pressure gradient. In such cases, a foam model can represent a trigger for foam generation.

We cannot say conclusively whether or not the model of Chen et al. (2010) can represent a trigger for foam generation for any parameter values. Instead, we define criteria that must be satisfied if a trigger for foam generation is to be represented in this model. This family of models wasn't originally intended to include a threshold velocity/pressure gradient for foam generation (Kovscek and Radke, 1993).

The STARS simulator can represent a minimum velocity for foam propagation at the condition for foam collapse u_t^{col}, but not a separate criterion for propagation. The Population-Balance models of Kam and Rossen (2003) and Kam (2008) can represent threshold velocities for both foam generation and propagation at steady flow, because they include the dynamics of convection, creation and destruction of foam in relation to local pressure gradient and water saturation. In implicit-texture (IT) foam models, such as the foam model in STARS, foam itself is not transported, in the absence of an explicit definition of foam texture as a component in the model. In IT models, creation and propagation of foam can happen upon achieving sufficient local pressure gradient as evaluated numerically by the simulator.

Our results suggest a serious problem for all foam models where foam generation is based on pressure gradient in conventional simulation with relatively large grid blocks: superficial velocity and pressure gradient at the well are not represented explicitly. Foam generation at the wellbore would not be represented without truly extraordinary grid resolution near the well. Simulations of linear displacements or of radial flow with extraordinarily fine grid refinement can still provide valuable insights into foam mechanisms that affect behavior on a larger scale.

Declaration of competing interest

The authors declare that they have no known competing financial interests or personal relationships that could have appeared to influence the work reported in this paper.

Acknowledgement

We are grateful to the sponsors (Shell, Equion, Engie, ConocoPhillips and PEMEX) of the Joint Industry Project (JIP) on Foam for Enhanced Oil Recovery at Delft University of Technology for their support. We also thank V.C. Chandrasekar (Computer Modeling Group-CMG) for his valuable discussions of and insights into the STARS simulation of radial foam propagation. Many thanks to Prof. A.R. Kovscek for checking our analysis of the model of Chen et al. (2010). In addition, we thank Dr. Sebastien Vincent-Bonnieu (ESA) and Dr. Xiaocong Lyu (Delft University of Technology) for their assistance and support.

Appendix A. Parameter values for foam models

Table A1
Population-Balance model of Kam and Rossen (2003).

Foam parameters (Kam and Rossen, 2003)		Other parameters (Kam and Rossen, 2003)	
C_g/C_c	1×10^{-13}	k [m^2]	7.1×10^{-12}
C_f	1×10^{-14}	φ	0.199
m	4.4	μ_w [Pa s]	0.001
n	0.85	μ_g [Pa s]	0.00002
S_w*	0.22	S_{wc}	0.2
		S_{gr}	0.1
		k^0_{rw}	0.7888
		k^0_{rg}	1.0
		n_w	1.9575
		n_g	2.2868

Table A2
Population-Balance model of Kam (2008).

Foam parameters (Kam, 2008)		Other parameters (Kam, 2008)	
C_g/C_c	3.6×10^{16}	k [m^2]	30.4×10^{-12}
C_c	1	φ	0.31
C_f	1.535×10^{-16}	μ_w [Pa s]	0.001
∇P0 [Pa/m]	9.5×10^4	μ_g [Pa s]	0.00002
n	1.0	S_{wc}	0.04
S_w*	0.0585	S_{gr}	0.0
n_f* [m^{-3}]	8×10^{13}	k^0_{rw}	0.7888
		k^0_{rg}	1.0
		n_w	1.9575
		n_g	2.2868

Table A3
STARS implicit-texture foam model (Computer Modeling Group, 2017). Parameter values are from Lotfollahi et al. (2017).

Foam parameters	Value Lotfollahi et al. (2017)	Other parameters	Steady-state model (Figs. 8 and 9) Lotfollahi et al. (2017)	Simulation (Fig. 12)
fmmob	85,700	k [m^2]	7.2×10^{-12}	10×10^{-12}
fmgcp	4.2×10^{-5}	φ	0.199	0.199
epgcp	1.5	k^0_{rw}	0.15	0.15
fmcap	2.46×10^{-5}	k^0_{rg}	1.0	0.8
epcap	0.5	n_w	1.95	1.9575
sfdry (fmdry)	0.22	n_g	2.28	2.2868
sfbet (epdry)	100	S_{wc}	0.2	0.2
		S_{gr}	0.1	0.0
		σ [N/m]	0.03	0.03 (independent of reservoir temperature)

Table A4
Implicit-texture foam model Lotfollahi et al. (2017).

Foam parameters	Value Lotfollahi et al. (2016)	Other parameters	Steady-state model (Figs. 10 and 11) Lotfollahi et al. (2016)
Fmmob	85,700	k [m^2]	7.2×10^{-12}
Fmgcp	4.2×10^{-5}	φ	0.199
epgcp	1.5	k^0_{rw}	0.15
fmcap	2.46×10^{-5}	k^0_{rg}	1.0
epcap	0.5	n_w	1.95
sfdry (fmdry)	0.22	n_g	2.28
sfbet (epdry)	100	S_{wc}	0.2
Ncamax	4.7×10^{-4}	S_{gr}	0.1
fgenc	0.0	σ [N/m]	0.03

References

Alvarez, J., Rivas, H., Rossen, W.R., 2001. Unified model for steady-state foam behavior at high and low foam qualities. SPE J. 6 (3) https://doi.org/10.2118/74141-PA, 325-222.

Apaydin, O.G., Kovscek, A.R., 2001. Surfactant concentration and end effects on foam flow in porous media. Transport Porous Media 43, 511–536. https://doi.org/10.1023/A:1010740811277.

Ashoori, E., Marchesin, D., Rossen, W.R., 2012. Multiple foam states and long-distance foam propagation in porous media. SPE J. 17 (4), 1231–1245. https://doi.org/10.2118/154024-PA.

Blaker, T., Aarra, M.G., Skauge, A., Rasmussen, L., Celius, H.K., Martinsen, H.A., Vassenden, F., 2002. Foam for gas mobility control in the Snorre field: the FAWAG project. SPE Reservoir Eval. Eng. 5 (4), 317–323. https://doi.org/10.2118/78824-PA.

Chen, Q., Gerritsen, M.G., Kovscek, A.R., 2010. Modeling foam displacement with the local-equilibrium approximation: theory and experimental verification. SPE J. 15 (1), 171–183. https://doi.org/10.2118/116735-PA.

Cheng, L., Reme, A.B., Shan, D., Coombe, D.A., Rossen, W.R., 2000. Simulating foam processes at high and low foam qualities. In: Paper Presented at the SPE/DOE Improved Oil Recovery Symposium. https://doi.org/10.2118/59287-MS. Tulsa, Oklahoma, April 2000.

Chou, S., 1991. Conditions for generating foam in porous media. In: Paper Presented at the SPE Annual Technical Conference and Exhibition. https://doi.org/10.2118/22628-MS. October 6–9, 1991.

Computer Modeling Group, STARS User's Guide, Version 2017.10, (Calgary, Alberta, Canada).

Falls, A.H., Hirasaki, G.J., Patzek, T.W., Gauglitz, D.A., Miller, D.D., Ratulowski, T., 1988. Development of a Mechanistic Foam Simulator: the Population Balance and Generation by Snap-Off. SPE J. https://doi.org/10.2118/14961-PA.

Friedmann, F., Chen, W.H., Gauglitz, P.A., 1991. Experimental and simulation study of high-temperature foam displacement in porous media. SPE J. 6 (1), 37–45. https://doi.org/10.2118/17357-PA.

Friedmann, F., Smith, M.E., Guice, W.R., Gump, J.M., Nelson, D.G., 1994. Steam-foam mechanistic field trial in the midway-sunset field. SPE J. 9 (4), 297–304. https://doi.org/10.2118/21780-PA.

Gauglitz, P.A., Friedmann, F., Kam, S.I., Rossen, W.R., 2002. Foam generation in homogeneous porous media. J Chem. Eng. Sci. 57 (19), 4037–4052. https://doi.org/10.1016/S0009-2509(02)00340-8.

Izadi, M., Kam, S.I., 2019. Bubble-population-balance modeling for supercritical carbon dioxide foam enhanced-oil-recovery processes: from pore-scale to core-scale and field-scale events. SPE Reservoir Eval. Eng. 22 (4), 1467–1480. https://doi.org/10.2118/191202-PA.

Izadi, M., Nguyen, P.H., Fleifel, H., Maestre, D.O., Kam, S.I., 2021. An investigation of mechanistic foam modeling of optimum field development of CO_2 foam EOR application. SPE Reservoir Eval. Eng. 24 (3), 475–494. https://doi.org/10.2118/205494-PA.

Kam, S.I., Rossen, W.R., 2003. A model for foam generation in homogeneous media. SPE J. 8 (4), 417–442. https://doi.org/10.2118/87334-PA.

Kam, S.I., Nguyen, Q.P., Li, Q., Rossen, W.R., 2007. Dynamic simulations with an improved model for foam generation. SPE J. 12 (1) https://doi.org/10.2118/90938-PA, 35-28.

Kam, S.I., 2008. Improved mechanistic foam simulation with foam Catastrophe theory. J Coll & Surf A 318 (1–3), 62–77. https://doi.org/10.1016/j.colsurfa.2007.12.017.

Khatib, Z.R., Hirasaki, G.J., Falls, A.H., 1988. Effects of capillary pressure on coalescence and phase mobilities in foams flowing through porous media. SPE J. 3 (3), 919–926. https://doi.org/10.2118/15442-PA.

Kovscek, A.R., Radke, C.J., 1993. Fundamentals of Foam Transport in Porous Media. https://doi.org/10.2172/10192736. United States: N. P.

Kovscek, A.R., Radke, C.J., 1994. Fundamentals of foam transport in porous media. In: Schramm, L.L. (Ed.), Foams: Fundamentals and Applications in the Petroleum Industry. Washington DC: ACS Advances in Chemistry Series No. 242. Am. Chem. Soc.

Kovscek, A.R., Patzek, T.W., Radke, C.J., 1995. A mechanistic population balance model for transient and steady-state foam flow in Boise sandstone. Chem. Eng. Sci. 50 (23), 3783–3799. https://doi.org/10.1016/0009-2509(95)00199-F.

Kovscek, A.R., Radke, C.J., 1996. Gas bubble snap-off under pressure-driven flow in constricted noncircular capillaries. Colloids Surf., A: Physicochem. Engng Aspects 117, 55–76. https://doi.org/10.1016/0927-7757(96)03637-0.

Kovscek, A.R., Bertin, H.J., 2003. Foam mobility in heterogeneous porous media. In: Transport in Porous Media, vol. 52, pp. 37–49. https://doi.org/10.1023/A:1022368228594.

Kuehne, D.L., Ehman, D.I., Emanuel, A.S., Magnani, C.F., 1990. Design and evaluation of a nitrogen-foam field trial. J. Petrol. Technol. 42 (2), 504–512. https://doi.org/10.2118/17381-PA.

Lee, W., Lee, S., Izadi, M., Kam, S.I., 2016. Dimensionality-dependent foam rheological properties: how to go from linear to radial geometry for foam modeling and simulation. SPE J. 21 (5), 1669–1687. https://doi.org/10.2118/175015-PA.

Leverett, M.C., 1941. Capillary behavior in porous solids. Trans. AIME 142 (1), 152–169. https://doi.org/10.2118/941152-G.

Lotfollahi, M., Farajzadeh, R., Delshad, M., Varavei, A., Rossen, W.R., 2016. Comparison of implicit-texture and population-balance foam models. J. Nat. Gas Sci. Eng. 31, 184–197. https://doi.org/10.1016/j.jngse.2016.03.018.

Lotfollahi, M., Kim, I., Beygi, M.R., Worthen, A.J., Huh, C., Johnston, K.P., Wheeler, M. F., DiCarlo, D.A., 2017. Experimental studies and modeling of foam hysteresis in porous media. Transport Porous Media 116, 687–703. https://doi.org/10.2118/179664-MS.

Ma, K., Lopez-Salinas, J.L., Puerto, M.C., Miller, C.A., Biswal, S.L., Hirasaki, G.J., 2013. Estimation of parameters for the simulation of foam flow through porous media. Part 1: the dry-out effect. Energy Fuels 27 (5), 2363–2375. https://doi.org/10.1021/ef302036s.

Martinsen, H., Vassenden, F., 1999. Foam assisted water alternating gas (FAWAG) process on snorre. In: 10th European Symposium on Improved Oil Recovery. https://doi.org/10.3997/2214-4609.201406335. Brighton, UK.

Moradi-Araghi, A., Johnston, E.L., Zornes, D.R., Harpole, K.J., 1997. Laboratory evaluation of surfactants for CO_2-foam applications at the South Cowden unit. In: Paper Presented at the International Symposium on Oilfield Chemistry. https://doi.org/10.2118/37218-MS. Houston, Texas, Feb 1997.

Patzek, T.W., 1996. Field Applications of Steam Foam for Mobility Improvement and Profile Control. Society of Petroleum Engineers. https://doi.org/10.2118/29612-PA.

Peaceman, D.W., 1978. Interpretation of well-block pressures in numerical reservoir simulation. SPE J. 18 (3), 183–194. https://doi.org/10.2118/6893-PA.

Ransohoff, B.T.C., Radke, C.J., 1988. Mechanisms of foam generation in glass-bead packs. SPERE 3 (2), 573–585. https://doi.org/10.2118/15441-PA.

Roof, J.G., 1970. Snap-off of oil droplets in water-wet pores. J. Soc. Petrol. Eng. SPE J. 10 (1), 85–90. https://doi.org/10.2118/2504-PA. Mar 1970.

Rossen, W.R., 1996. Foams in enhanced oil recovery. Chap. 11. In: Prud'homme, R.K., Khan, S. (Eds.), Foams: Theory, Measurements, and Applications, Surfactant Science Series, vol. 57. Marcel Dekker, Inc. 270 Madison Avenue, New York, 10016.

Rossen, W.R., Gauglitz, P.A., 1990. Percolation theory of creation and mobilization of foams in porous media. J. AIChE 36 (8), 1176–1188. https://doi.org/10.1002/aic.690360807.

Schramm, L.L., 1994. Foams: fundamentals and applications in the petroleum industry. In: Washington DC: ACS Advances in Chemistry Series No. 242. Am. Chem. Soc.

Simjoo, M., Nguyen, Q.P., Zitha, P.L.J., L J, P., 2012. Rheological transition during foam flow in porous media. Ind. Eng. Chem. Res. 51, 10225–10231. https://doi.org/10.1021/ie202218z.

Tang, G., Kovscek, A.R., 2006. Trapped gas fraction during steady-state foam flow. Transport Porous Media 65 (2), 287–307. https://doi.org/10.1007/s11242-005-6093-4.

Yu, G., Rossen, W.R., Vincent-Bonnieu, S., 2019. Coreflood study of effect of surfactant concentration on foam generation in porous media. J. I EC 58 (1), 420–427. https://doi.org/10.1021/acs.iecr.8b03141.

Yu, G., Vincent-Bonnieu, S., Rossen, W.R., 2020. Foam propagation at low superficial velocity: implications for long-distance foam propagation. SPE J. 25 (6), 3457–3471. https://doi.org/10.2118/201251-PA.

Zeeman, E.C., 1977. Catastrophe theory. Sci. Am. 234 (4) (April 1976): 65-83 65-83. https://www.jstor.org/stable/24950329.

Nomenclature

Symbol Definition

C_s: Surfactant concentration
f_g: Foam quality
k: Permeability
k_{rg}: Relative permeability of gas
k_{rg}^f: Gas relative permeability in presence of foam
k_{rw}: Relative permeability of water
n_f: Foam texture (or lamella/bubble density)
P: Pressure
P_c: Capillary pressure
$P_c{}^*$: Limiting capillary pressure
∇P: Pressure gradient
ΔP: Pressure difference
∇P^{gen}: Minimum/threshold pressure gradient for foam generation
r_g: Rate of lamella creation
r_c: Rate of lamella coalescence
S_g: Gas saturation
S_{gr}: Residual gas saturation
S_w: Water saturation
S_{wc}: Connate water saturation
$S_w{}^*$: Limiting water saturation
u_t: Total superficial velocity
u_w: Water superficial velocity
u_g: Gas superficial velocity
u_t^{gen}: Minimum/threshold superficial velocity for foam generation
u_t^{prop}: Minimum/threshold superficial velocity for foam propagation
u_t^{col}: Minimum/threshold superficial velocity for foam collapse
v_w: Water interstitial velocity

v_g: Gas interstitial velocity
φ: porosity
μ_w: Viscosity of water
μ_g: Viscosity of gas

Conversion Factors: SI Units to Common Oilfield Units

2.26×10^4 Pa m^{-1}: 1 psi ft^{-1}
3.52×10^{-6} m s^{-1}: 1 ft day^{-1}
9.84×10^{-8} $(m^2$ (Pa s)$^{-1})$: 1 md cp^{-1}
10^5 Pa: 1 bar

Guanqun Yu obtained his PhD degree from Delft University of Technology. He holds an MSc degree in Petroleum Engineering from Delft University of Technology, and a BSc degree in Geographical Information System and Remote Sensing from Jilin University, China. His current research interests include foam generation and propagation in homogeneous porous media.

William Rossen is Professor Emeritus of Reservoir Engineering in the Department of Geoscience and Engineering at Delft University of Technology. His research focuses on generation and flow of foam in porous media and fractures for EOR purpose, sweep efficiency and injectivity of gas EOR, fractional-flow theory for complex chemical EOR, and modeling and simulation of foam and chemical EOR.